Possible charge disproportionation in $3R$-$AgNiO_2$ studied by neutron powder diffraction

J.-H. Chung,[1,*] J.-H. Lim,[2] Y. J. Shin,[2] J.-S. Kang,[3] D. Jaiswal-Nagar,[4] and K. H. Kim[4]
[1]*Department of Physics, Korea University, Seoul 136-713, Korea*
[2]*Department of Chemistry, The Catholic University of Korea, Bucheon 420-743, Korea*
[3]*Department of Physics, The Catholic University of Korea, Bucheon 420-743, Korea*
[4]*Department of Physics and Astronomy & FPRD, Seoul National University, Seoul 151-747, Korea*
(Received 29 May 2008; revised manuscript received 24 September 2008; published 11 December 2008)

Using neutron-scattering techniques, we have investigated the nuclear and the magnetic structures of the triangular antiferromagnet $3R$-$AgNiO_2$. The symmetry analysis based on the group theory suggests that the $\sqrt{3}\times\sqrt{3}$ charge order proposed for $2H$-$AgNiO_2$ [E. Wawrzyńska *et al.*, Phys. Rev. Lett. **99**, 157204 (2007)] will have a monoclinic symmetry if present in the trigonal lattice of $3R$-$AgNiO_2$. The Rietveld refinement shows that symmetry reduction in the NiO_2 layer is consistent with the prediction of the group theory. The pair density function consistently shows that the nearest-neighbor Ni-O bonds split into two groups separated by approximately 0.1 Å. The antiferromagnetic Bragg peaks observed below $T_N=25$ K can be described by the propagation vector $\mathbf{k}=(0,1,0)$ of the monoclinic unit cell. The similarities of the local structure and the antiferromagnetic order strongly suggest that the novel charge order observed in $2H$-$AgNiO_2$ also exists in $3R$-$AgNiO_2$.

DOI: 10.1103/PhysRevB.78.214417 PACS number(s): 75.25.+z, 61.05.F−, 75.50.Ee

I. INTRODUCTION

Transition-metal oxides with triangular lattice symmetry are an interesting class of material because strong electron correlations can occur on the geometry that is subject to frustration. Unusual properties are observed especially when the transition-metal ions have partially occupied electronic orbitals.[1–11] Among them, delafossite oxides containing Ni^{3+} ions are good examples to observe rich and complex magnetic properties.[4–11] In these materials, each magnetic Ni^{3+} ion ($t_{2g}^6 e_g^1$) is surrounded by six oxygen ions, and the threefold symmetry is established among three tilted octahedra sharing a vertex. Therefore, their lattices provide possibilities not only for magnetic but even charge or orbital frustrations, leading to various forms of electronic and/or magnetic order. $NaNiO_2$ is the simplest case showing antiferromagnetic stacking of ferromagnetic NiO_2 layers.[4,5] Its structural symmetry is monoclinic due to the ferro-orbital order of the Jahn-Teller active Ni^{3+} ions. In contrast, $LiNiO_2$ shows no long-range magnetic transitions in spite of the apparent local Jahn-Teller effect,[6,7] and the nature of its magnetism is controversial from frustrated antiferromagnetism to orbital liquids.[8–11] The absence of long-range magnetic order has recently been explained by trimer orbital order that maintains the threefold symmetry of the lattice.[7]

When the electrons are more delocalized, on the other hand, Jahn-Teller effect is suppressed and charge disproportionation may be observed. For instance, coexistence between Ni ions of two different electronic states is observed in semimetallic delafossite $3R$-$AgNiO_2$.[12] Interestingly, a novel $\sqrt{3}\times\sqrt{3}$ charge order was recently observed in the hexagonal analog, $2H$-$AgNiO_2$, by neutron diffraction.[13,14] This charge order is accompanied by an in-plane antiferromagnetic order of Ni^{2+} spins that is established via Ni-O-O-Ni superexchange. In comparison, such reduction in lattice symmetry due to electronic inhomogeneity is yet to be reported for $3R$-$AgNiO_2$ although it has been more widely studied. Therefore, it naturally raises a question whether or not a similar charge order is also present in $3R$-$AgNiO_2$.

In this paper, we report our neutron-scattering investigation of the structure and the magnetism of the triangular antiferromagnetic delafossite $3R$-$AgNiO_2$. Based on the group theory, we find that the proposed charge order will cause monoclinic distortion in $3R$-$AgNiO_2$. The Rietveld and the pair density function (PDF) refinements using a monoclinic structural model show that the oxygen sublattice distorts in ways consistent with the proposed charge order. We also find that its antiferromagnetic transition observed at $T_N=25$ K has the characteristic ordering wave vector that is consistent with the symmetry of the charge order. These results strongly suggest that the novel charge order proposed for $2H$-$AgNiO_2$ may also exist in $3R$-$AgNiO_2$.

II. EXPERIMENT

Powder samples (≈4 g) of $3R$-$AgTO_2$ (T=Ni and Fe) were synthesized by cation exchange of $NaNiO_2$, which was originally synthesized via solid-state reaction as described previously.[15] Neutron powder diffraction measurement for structural analysis were performed using the NPDF time-of-flight neutron diffractometer at the Lujan Neutron Scattering Center of the Los Alamos National Laboratory. The collected diffraction profiles were analyzed by the Rietveld refinement method using the GSAS program.[16] For local structural studies, we converted the neutron diffraction intensities to the normalized structure function, $S(Q)$, from which the neutron pair density functions, $G(r)$, were obtained by the following relation:[17]

$$G(r) = \int_0^\infty Q[S(Q) - 1]\sin(Qr)dQ. \quad (1)$$

The model calculations and the refinements of the neutron PDFs were performed using the DIFFPY program.[18]

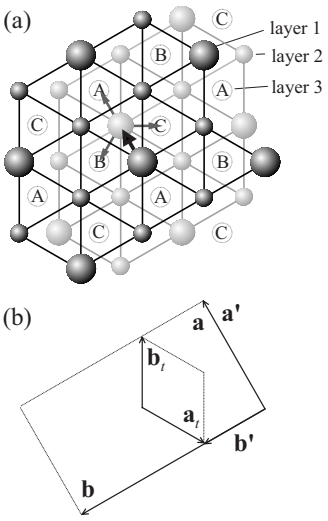

FIG. 1. (a) Top view of the three NiO_2 layers in $3R$-$AgNiO_2$. In each layer, large and small spheres represent charge-rich (Ni1) and charge-poor (Ni2) sites, respectively, of the proposed $\sqrt{3}\times\sqrt{3}$ order. (b) The relation between the basal planes of the trigonal ($\mathbf{a}_t\times\mathbf{b}_t$) and the monoclinic ($\mathbf{a}\times\mathbf{b}$) unit cells of $3R$-$AgNiO_2$. Also shown in the basal plane of the $NaNiO_2$ unit cell ($\mathbf{a}\times\mathbf{b}'$).

The magnetic Bragg reflections were observed using two constant-wavelength neutron-scattering instruments of the NIST Center for Neutron Research. The measurement at the BT1 powder diffractometer was done using the neutrons of wavelength $\lambda=2.087$ Å. Temperature dependences of the selected magnetic Bragg peaks were measured at the Spin-Polarized Inelastic Neutron Spectrometer (SPINS) using the neutrons of wavelength $\lambda=4.879$ Å. For the latter, two Be filers were used to remove contaminations from higher-order neutrons.

III. RESULTS AND DISCUSSION

A. Symmetry analysis for charge order

A unit cell of $2H$-$AgNiO_2$ has two NiO_2 layers, on which the Ni ions occupy the same in-plane fractional coordinates, i.e., $(x,y,z)=(0,0,0)$ and $(0,0,\frac{1}{2})$, respectively. In contrast, a unit cell of $3R$-$AgNiO_2$ has three NiO_2 layers, and its Ni ions occupy different in-plane fractional coordinates from each other. Therefore, stacking of the $\sqrt{3}\times\sqrt{3}$ ordered NiO_2 layers will have different choices between the two polymorphs. Figure 1 shows the three Ni layers in $3R$-$AgNiO_2$ seen from the direction parallel to the c axis. In this structure, any choices of electron rich (Ni1) sites on two adjacent layers are equivalent because every Ni ion in one plane has three nearest Ni ions at equal distances on an adjacent plane. One of the six equivalent choices between layers 1 and 2 is shown in Fig. 1. It is in fact the choices on layer 3 that will produce three different stacking patterns. The choice of the site A in Fig. 1 will produce linear chains that are tilted off the c axis. On the other hand, the site B (C) will produce left (right)-handed spirals instead. From structure factor calculations we find that in all of the cases the propagation vector is commonly $\mathbf{k}=(\frac{1}{3},\frac{1}{3},0)$. An analysis based on the group theory shows, however, that only one among the three choices is compatible with the symmetry of the $R\bar{3}m$ space group.[19] For the given space group and the propagation vector, there is only one basis vector of the irreducible representation for charge order on Ni sites. (See Table I.) This basis vector can only produce linear chains that are perpendicular to the propagation vector, for instance, such as the one connecting Ni1 ions on $(x,y,z)=(-\frac{1}{3},\frac{1}{3},\frac{5}{6})$, $(0,0,\frac{1}{2})$, and $(\frac{1}{3},-\frac{1}{3},\frac{1}{6})$. Compatible oxygen displacements can also be explained by the group theory. Among the basis vectors of the irreducible representations for displacement order at the oxygen sites listed in Table II, we find that the displacements similar to those observed in $2H$-$AgNiO_2$ (Ref. 13) can be reproduced by a linear combination of the two vectors, i.e., $-e^{i\pi/3}\tau_1^1+\tau_1^2$. The corresponding oxygen displacements are shown in Fig. 2. In contrast, the displacements compatible for two other spiral stacking patterns are not reproduced by any combinations.

TABLE I. Basis vectors for the irreducible representations for scalar mode (charger order) at the Ni sites in space group $R\bar{3}m$ for the propagation vector $\mathbf{k}=(\frac{1}{3},\frac{1}{3},0)$.

Position	(1/3, 2/3, 1/6)	(0, 0, 1/2)	(2/3, 1/3, 5/6)
Γ_1	$e^{i2\pi/3}$	1	$e^{i2\pi/3}$

The above analysis implies that lowering of symmetry due to the proposed charge order should be quite different between the two polymorphs. In $2H$-$AgNiO_2$, the charge order changes the structural space group from $P6_3/mmc$ to $P6_322$.[14] As a result, its unit cell is expanded by $\sqrt{3}\times\sqrt{3}$ but still maintains hexagonal symmetry. In $3R$-$AgNiO_2$, in con-

TABLE II. Basis vectors for the irreducible representations for polar mode (displacement) at the oxygen sites in space-group $R\bar{3}m$ for the propagation vector $\mathbf{k}=(\frac{1}{3},\frac{1}{3},0)$. ($p=e^{i2\pi/3}$, $q=e^{i5\pi/3}$.)

Position	$(0,0,\frac{1}{6}-z_O)$	$(\frac{2}{3},\frac{1}{3},\frac{1}{6}+z_O)$	$(\frac{2}{3},\frac{1}{3},\frac{1}{2}-z_O)$	$(\frac{1}{3},\frac{2}{3},\frac{1}{2}+z_O)$	$(\frac{1}{3},\frac{2}{3},\frac{5}{6}-z_O)$	$(0,0,\frac{5}{6}+z_O)$
τ_1^1	(1,1,0)	$(p,p,0)$	$(p,p,0)$	$(p,p,0)$	$(p,p,0)$	(1,1,0)
τ_1^2	(0,1,0)	$(p,0,0)$	$(0,p,0)$	$(p,0,0)$	$(0,p,0)$	(1,0,0)
τ_1^3	(0,0,1)	$(0,0,p)$	$(0,0,q)$	$(0,0,p)$	$(0,0,q)$	$(0,0,-1)$
τ_2^1	(1,1,0)	$(q,q,0)$	$(p,p,0)$	$(q,q,0)$	$(p,p,0)$	$(-1,-1,0)$
τ_2^2	(0,1,0)	$(q,0,0)$	$(0,p,0)$	$(q,0,0)$	$(0,p,0)$	$(-1,0,0)$
τ_2^3	(0,0,1)	$(0,0,p)$	$(0,0,p)$	$(0,0,p)$	$(0,0,p)$	(0,0,1)

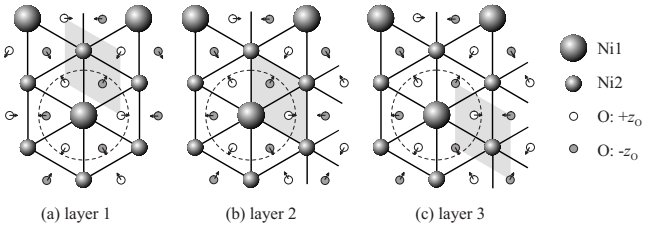

FIG. 2. The expected oxygen displacements in the case of $\sqrt{3} \times \sqrt{3}$ charge order that is consistent with the basis vector Γ_1 in Table I. The gray shaded areas represent the $R\bar{3}m$ unit cell.

trast, it is apparent that formation of the chains will remove threefold symmetry elements of the $R\bar{3}m$ space group and effectively induce a shear stress. As a result, the lattice symmetry will become monoclinic instead of remaining as trigonal. A similar symmetry reduction from $R\bar{3}m$ down to a monoclinic space group has been well known in the case of orbital-ordered $NaNiO_2$.[20] In this material, ferro-orbital order of Ni^{3+} ($3d^7$) breaks the symmetry among the interplane Ni-Ni distances and stabilizes the $C2/m$ structure. A monoclinic distortion in 3*R*-$AgNiO_2$ is expected to be in the same direction since it should be due to Coulomb repulsion between Ni1 ions but probably much smaller in magnitude.

In the following sections, we experimentally test the possibility of the expected symmetry reduction. We choose to use the structure based on space-group $C2/m$. Since there are two types of Ni sites,[21] however, we consider a unit cell three times larger than the unit cell of $NaNiO_2$. The relations between the unit cells in the basal planes are shown in Fig. 1(b).

B. Nuclear structures

Figure 3(a) shows the neutron powder diffraction profile collected at $T=10$ K and the calculated profiles based on the nominal $R\bar{3}m$ space group. While the experimental intensity is reasonably well reproduced by the calculation, mismatch of the (1,0,10) reflection intensity ($Q=4.22$ Å^{-1}) is easily noticed. In comparison, the experimental and the calculated profiles of 3*R*-$AgFeO_2$ in Fig. 3(c) show an excellent agreement with each other. From visual inspections alone, however, it was not clear whether or not any superlattice peaks exist in 3*R*-$AgNiO_2$ that may be associated with the expected lattice symmetry reduction. The diffraction profiles are essentially featureless and do not show much temperature dependence below 300 K. We have performed Rietveld refinement using the $C2/m$ structure and compared with the experimental data. The best-fit structural parameters are listed in Table III, and the calculated profile is plotted in Fig. 3(b). We find that the obtained structure is consistent with the proposed charge order and the difference between the average shorter and the average longer nearest-neighbor (NN) Ni-O bond distances is approximately 0.1 Å. While the overall agreement was improved by the monoclinic structure, it also showed that calculated intensities of the superlattice peaks are weaker than the primary peaks by more than 2 orders of magnitude. Unfortunately, our data contained intensities from diffusive background (subtracted and not shown in Fig. 3) and small amount of impurity, which practically prevented us from unambiguously observing the superlattice peaks.

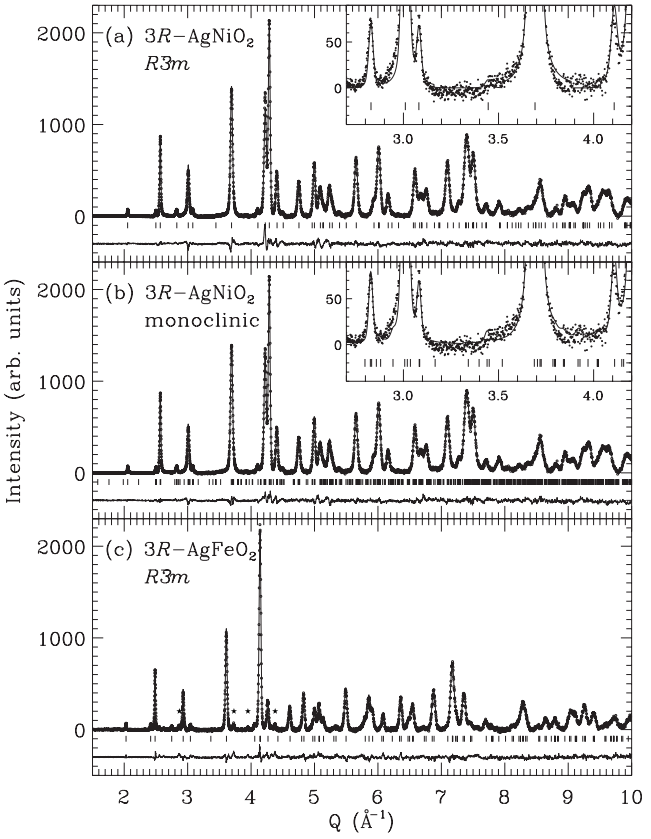

FIG. 3. Experimental (open dots) and calculated (solid lines) neutron powder diffraction profiles and their differences of 3*R*-$AgNiO_2$(a,b) and 3*R*-$AgFeO_2$ at $T=10$ K. The profiles were calculated based on [(a) and (c)] the nominal $R\bar{3}m$ model or (b) the monoclinic $C2/m$ model. The vertical marks represent the Bragg peak positions, and the star symbols are the impurity peaks. The insets show the region where superlattice peaks are expected for the monoclinic structure.

In order to further search for the evidence of lattice distortions, we have converted the neutron diffraction profile into the PDF using Eq. (1) and plotted in Figs. 4 and 5. The overall PDF is moderately reproduced by the model calculation based on the $R\bar{3}m$ unit cell. However, a close inspection of the experimental PDF indeed suggested an important signature of the symmetry reduction on the oxygen sublattice. The NN peak at $r \approx 2$ Å consists mainly of the shortest Ni(Fe)-O distances. Figures 4(a) and 5(a) show that the experimental NN peak is broad and noticeably asymmetric for 3*R*-$AgNiO_2$. In contrast, the experimental NN peak of 3*R*-$AgFeO_2$ is relatively sharp and quite symmetric as shown in Fig. 5(c). This is a good signature that there are more than one NN Ni-O bond distances and the symmetry of the NiO_2 layer is reduced with respect to the ideal structure. In comparison, the Ni-Ni ($r=2.94$ Å) and the Fe-Fe ($r=3.03$ Å) peaks are both symmetric and equally narrow. We note that both delafossites have the shortest Ag-O distances at 2.08 Å,

TABLE III. The best fit parameters obtained from the model fitting at $T=10$ K based on the monoclinic $C2/m$ model. The atomic positions are Ag1:$(0,\frac{1}{2},\frac{1}{2})$, Ag2:$(0,y,\frac{1}{2})$, Ni1:(0,0,0), Ni2:$(0,y,0)$, O1:$(x,0,z)$, and O2:$(x,y,z)$. A constraint was used between O1(z) and O2(z).

	Rietveld	PDF
a (Å)	5.0697(2)	5.078(2)
b (Å)	8.7953(4)	8.795(6)
c (Å)	6.3524(2)	6.376(12)
β (deg)	105.732(4)	106.02(8)
Ag2(y)	0.1671(12)	0.1675(8)
Ni2(y)	0.3333(7)	0.3358(3)
O1(x)	0.4091(14)	0.4023(4)
O1(z)	0.1639(2)	0.1614(3)
O2(x)	0.3774(8)	0.3796(3)
O2(y)	0.3259(7)	0.3258(3)
O2(z)	0.1639(2)	0.1614(3)
	Average	
Ni1-O (Å)	2.045(3)	2.027(2)
Ni2-O (Å)	1.928(3)	1.929(2)

which interfere with the Ni/Fe-O peak. However, the overall shape of the peak did not change noticeably because the coherent scattering length of silver is relatively small.

Using the monoclinic structure that is previously tested, we have performed PDF refinement to see if the asymmetric shape of the observed NN peak profile can be reproduced. Figures 4(b) and 5(b) show that although the PDF is nearly unaffected at distances larger than the size of NiO_6 octahedra ($\gtrsim 4$ Å), the shape of the NN peak is substantially improved by the monoclinic model. The best-fit structural parameters are listed in Table III, which consistently show that the NN Ni-O bond distances split into two groups separated by ≈ 0.1 Å. In this structure, every one out of three NiO_6 octahedra is expanded while those surrounding contract.[13] As a result, the ratio between the weights of the shorter and the longer Ni-O bonds becomes exactly 2:1. This distribution of the NN bond distances is well accommodated into the experimentally observed PDF. In the bottom part of Figs. 5(a)–5(c) we also plotted the calculated partial PDFs for the Ni/Fe-O and the Ag-O bonds separately. When a single bond length is assumed, the Gaussian FWHM of the Ni-O peak becomes as large as 0.180 Å while that of the Fe-O peak is only 0.141 Å. Figure 5(d) also shows that the shape of the NN Ni-O peak clearly deviates from the symmetric Gaussian profile even after the Ag-O peak intensity is removed, indicating that there are more than one bond distances. Figure 5(e) shows that the asymmetry of the Ni-O peak persists at least up to 200 K.

The proposed monoclinic distortion, unless intentionally constrained, will produce three short and two long Ni-O bonds. The average short and long bond lengths obtained from the best-fit model are listed in Table III. Independently from the Rietveld and the PDF refinements, we obtain 1.93 and 2.03–2.04 Å for the shorter and the longer bonds, respectively. These values are very similar to the bond distances reported for $2H$-$AgNiO_2$.[13] This close agreement strongly suggests that our sample also possesses the mixture of two charge states similar to those in $2H$-$AgNiO_2$. The longer bond is ascribed to electron-rich and insulating Ni^{2+} (Ni1) ions, and the shorter bond is ascribed to electron-poor and metallic $Ni^{3.5+}$ (Ni2) ions. The ordering between the two species in $2H$-$AgNiO_2$ has been rationalized by energetic arguments based on Hund's rule energy gain.[13] Given the nearly identical symmetry of the NiO_2 layers, this argument will safely apply to $3R$-$AgNiO_2$ as well.

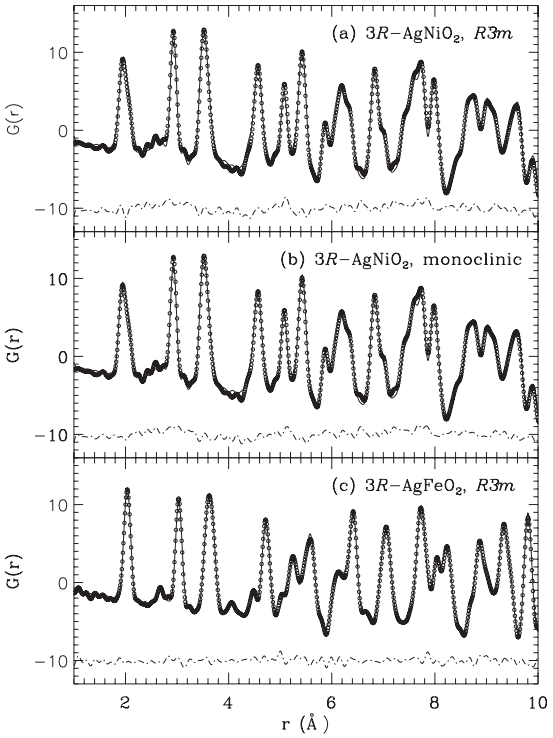

FIG. 4. Experimental (open circles) and calculated (solid lines) pair density functions of $3R$-$AgNiO_2$ [(a) and (b)] and $3R$-$AgFeO_2$ (c) at $T=10$ K. The profiles were calculated based on [(a) and (c)] the nominal $R\bar{3}m$ structure or (b) the monoclinic model with one third of NiO_6 octahedra expanded. The dash-dotted lines are the difference between the experimental and the calculated functions, which are displaced vertically for clarity.

We note that such asymmetric peak shape may also be observed from different structures. Examples are the ferro-orbital order of $NaNiO_2$ (Refs. 4 and 5) or the trimer orbital order of $LiNiO_2$.[7] In these structures, all of the NiO_6 octahedra are equally distorted due to the singly occupied e_g orbitals, producing the ratio 2:1 between the average shorter and the average longer Ni-O bonds. Although the PDF refinement is not sensitive enough to discriminate between our model and these two structures, we can rule them out based on other experimental findings. These alternative structures are commonly based on the uniform and localized electronic state of the Ni^{3+} ions. On the contrary, the mixed presence of the Ni ions with at least two different charge states has been explicitly observed in $3R$-$AgNiO_2$ by means of soft x-ray absorption spectroscopy.[12] This result strongly supports the

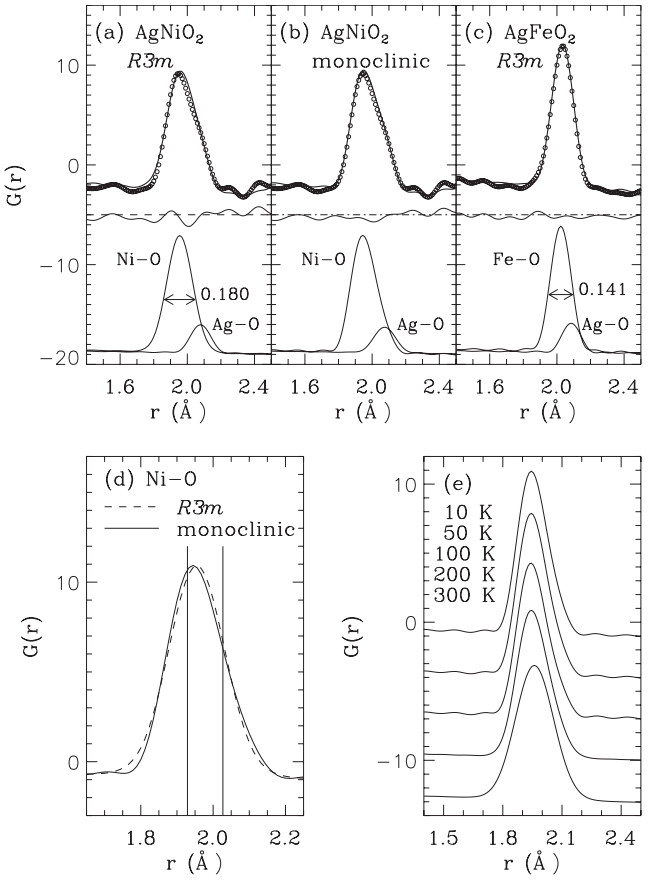

FIG. 5. [(a)–(c)] The nearest-neighbor peak in the experimental (open circles) and calculated (solid lines) pair density functions that are shown in Fig. 4. The lower parts show the calculated partial pair density functions for the Ni-O and the Ag-O pairs. (d) The Ni-O partial pair density functions calculated for the $R\bar{3}m$ (dashed lines) and the monoclinic (solid lines) models. The vertical lines mark the two average Ni-O bond distances obtained from the monoclinic model. (e) Temperature dependence of the calculated Ni-O partial pair density function.

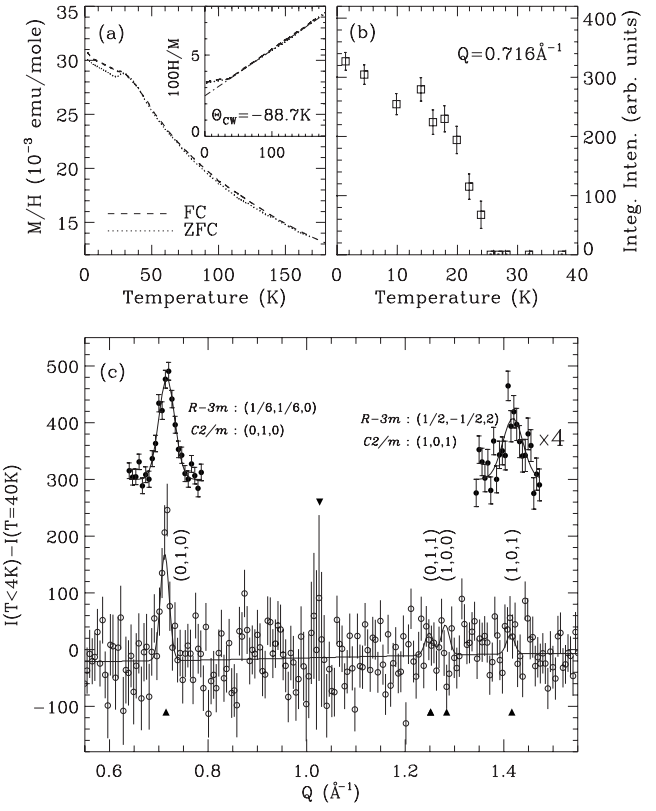

FIG. 6. (a) Low-field dc magnetization of $3R$-$AgNiO_2$ at $B=1$ T. The inset shows H/M and the linear fitting to the paramagnetic region. (b) Temperature dependence of the integrated intensity of the magnetic reflection at $Q=0.716$ Å^{-1}. (c) The difference intensity, $I(<4\text{ K})-I(40\text{ K})$, measured using the BT1 powder diffractometer (empty circles) and the SPINS triple axis spectrometer (filled circles), respectively. The solid line through the BT1 data is the calculation based on the model shown in Fig. 7(a). The filled downward and the upward triangles mark the positions of nuclear and magnetic Bragg peaks, respectively.

scenario that the two different Ni-O bond lengths do not belong to a single octahedron but to different octahedra. Such coexistence of two or more different charge states is also supported by the semimetallic conductivity previously reported for the same material.[15]

Even though there are some minor differences between the parameters obtained from the two refinement methods, they commonly show monoclinic structures consistent with the proposed $\sqrt{3}\times\sqrt{3}$ charge order. However, the magnitude of monoclinic distortion is relatively small. The tilt angle of the trigonal c_t axis due to the monoclinic distortion, $\theta=\sin^{-1}\{(a+3c\cos\beta)/|\mathbf{a}+3\mathbf{c}|\}$, is found in the range of 0.3–0.6° from either method. In contrast, it is as large as ≈1.9° for $NaNiO_2$. It is probably because the Coulomb repulsion between the Ni1 sites is screened by metallic conductivity. At the same time, contrary to Na^+ ions in $NaNiO_2$, Ag^+ ions in $3R$-$AgNiO_2$ are located at positions that can absorb the shear distortions. As a result, actual lattice distortions should be pretty much confined around NiO_6 octahedra. We note that such monoclinic symmetry should occur only if the coherence length along the c axis is larger than twice the spacing between the NiO_2 layers. Such large coherence will also be necessary in order for three-dimensional long-range magnetic structures to be stabilized.

C. Antiferromagnetic transition

The antiferromagnetic transition in $3R$-$AgNiO_2$ has been reported; but early attempts to observe magnetic Bragg peaks were unsuccessful and its magnetic structure has been unknown.[22] The low-field dc magnetization shows that our sample also undergoes antiferromagnetic transition at $T_N=25$ K. [See Fig. 6(a).] Using long-wavelength neutron diffraction we could successfully observe the antiferromagnetic transition but unambiguously identified only two magnetic Bragg peaks. Figure 6(c) shows the difference between the neutron diffraction intensities measured below and above T_N, respectively. The observed two peaks can be described using a single propagation vector, $\mathbf{k}=(0,1,0)$, based on the $C2/m$ unit cell that was used for structural analysis in Sec. III B. In contrast, they cannot be assigned a common propagation vector if the $R\bar{3}m$ unit cell is assumed. Therefore, the sym-

TABLE IV. Basis vectors for the irreducible representations for axial mode at the Ni sites in space group $C2/m$ for the propagation vector $\mathbf{k}=(0,1,0)$.

Position	(0,0,0)	(1/2,1/2,0)
Λ_1	$(0,u,0)$	$(0,-u,0)$
Λ_2^1	$(u,0,v)$	$(-u,0,-v)$
Λ_2^2	$(0,0,u)$	$(0,0,-u)$

metry of the antiferromagnetic structure is unlikely to be based on the $R\bar{3}/m$ space group. The transition temperature estimated from the temperature dependence of the magnetic Bragg peak at $Q=0.716$ Å^{-1} is in agreement with the dc magnetization data. [See Fig. 6(b).]

Based on the group theory, we find the spin arrangement must be antiferromagnetic within the *ab* plane but the symmetry would impose no constraints on the their orientations. (See Table IV.) However, we could approximately estimate the most probable spin orientation from the relatively intensities of the magnetic Bragg peaks. Our best-fit calculation that is shown as solid lines in Fig. 6(c) suggests that the spin orientation is almost perpendicular to the *ab* plane as shown in Fig. 7(a). This magnetic structure can be obtained by a linear combination of the two basis vectors of the irreducible representations Λ_2^1 and Λ_2^2 from Table IV. Although the accuracy of our data is not high enough to determine the exact spin orientation, the most probable antiferromagnetic structure obtained from our data is very similar to what has been observed in $2H$-$AgNiO_2$.

According to Wawrzyńska *et al.*,[13] the apparent interplanar ferromagnetic correlations between Ni1 ions in $2H$-$AgNiO_2$ can be explained by combining interplanar $J_\perp$(Ni1–Ni2) and intraplanar $J_\parallel$(Ni2–Ni1) that are both antiferromagnetic. They found that the $J_\perp$(Ni1–Ni2) was stronger than $J_\perp$(Ni1–Ni1) although Ni2 has a small ordered moment ($\lesssim 0.1\mu_B$). This explanation is also possible in $3R$-$AgNiO_2$ but only after careful considerations. It is important to be reminded that the major difference between the two structures is in the stacking patterns of Ni layers. In $2H$-$AgNiO_2$, the in-plane coordinates of the Ni ions are identical between the two different layers in a unit cell. [See Fig. 7(a).] However, the Ni1 sites are stacked in a staggered manner along the *c* axis due to the Coulomb repulsion. In this structure, the strength of a particular pairwise interaction will be determined by the total exchange path but not by the simple distance between the two ions. Therefore, the antiferromagnetic $J_\perp$(Ni1–Ni2) would be stabilized not because the Ni1-Ni2 distance is shorter but probably because it involves triple O-Ag-O bridges and shorter Ni2-O bonds. In comparison, $J_\perp$(Ni1–Ni1) involves a single O-Ag-O bridge and longer Ni1-O bonds only.

We realize that the situation is somewhat different in $3R$-$AgNiO_2$. In $3R$-$AgNiO_2$, a Ni site in one layer is located at the center of a triangle formed by three Ni sites on the adjacent layer. [See hatched areas in Fig. 7(b).] As a result, the Coulomb forces will no longer have much effect in determining the stacking pattern because one out of every three Ni sites on any layer should be occupied by Ni^{2+}. In this structure, both $J_\perp$(Ni1–Ni1) and $J_\perp$(Ni1–Ni2) equally involve double O-Ag-O bridges, which makes it very tempting to assume that the major interplanar exchange is ferromagnetic. However, there is no particular reason why the interplanar exchange through insulating Ag should be ferromagnetic. Instead, we find that as many as four antiferromagnetic $J_\perp$(Ni1–Ni2) can be satisfied simultaneously around one ferromagnetic $J_\perp$(Ni1–Ni1) for a particular structure, for instance, shown in Fig. 7(b). Therefore, it is probably the multiplicity of $J_\perp$(Ni1–Ni2) that stabilizes the apparent interplanar ferromagnetic correlations in $3R$-$AgNiO_2$. Theoretical works such as first-principles calculations may be able to provide more quantitative picture of the magnetic exchanges and eventually help us better understand the differences and similarities between the two polymorphs.

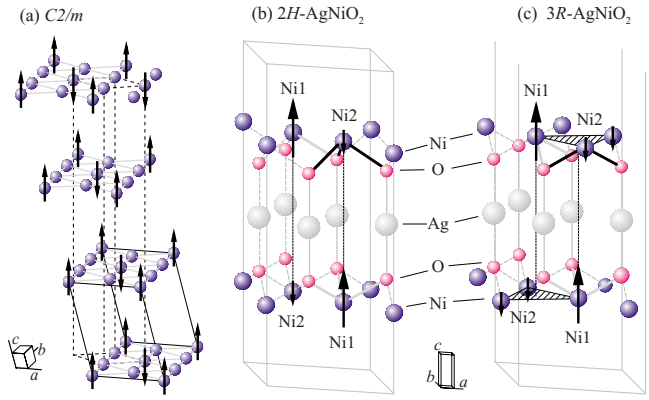

FIG. 7. (Color online) (a) The proposed antiferromagnetic structure of $3R$-$AgNiO_2$. The thick solid lines show the outline of the monoclinic unit cell. [(b) and (c)] Arrangements of two Ni layers in (a) $2H$-$AgNiO_2$ and (b) $3R$-$AgNiO_2$. In $3R$-$AgNiO_2$, the hatched areas are triangles formed by three Ni sites, whose centers coincide with the in-plane coordinates of Ni sites on the adjacent layers. Thick black lines indicate (the shorter) Ni2-O bonds while thick gray lines indicate (the longer) Ni1-O bonds. Other lines are guides to the eyes to find Ni-O or Ag-O bonds.

IV. SUMMARY AND CONCLUSIONS

In summary, we have studied the nuclear and the magnetic structures of the triangular antiferromagnetic $3R$-$AgNiO_2$ using neutron diffraction. If the $\sqrt{3}\times\sqrt{3}$ charge-ordered phase exists in $3R$-$AgNiO_2$, its symmetry is expected to be monoclinic by the group theory. The combination of the Rietveld and the PDF refinements provided structural signatures that are consistent with the presence of the proposed charge order. The difference between the average shorter and the average longer Ni-O bond distances is approximately 0.1 Å. We have also identified the long-range antiferromagnetic transition with the characteristic wave vector $\mathbf{k}=(0,1,0)$ in the monoclinic $C2/m$ unit cell. Based on these results, we argue that the $\sqrt{3}\times\sqrt{3}$ charge order proposed in the $2H$-$AgNiO_2$ may also exist in $3R$-$AgNiO_2$.

ACKNOWLEDGMENTS

The authors are grateful to Thomas Proffen and Qing Huang for their assistance during neutron diffraction experiments. This work was supported by the Korea Science and Engineering Foundation (KOSEF) grant funded by the Korea government (MEST) (No. R01-2008-000-10787-0), and also by the Nuclear R&D Programs (No. M20701050003-08N0105-00311). The work done at SNU was supported by the Korean Government through NRL program (Grant No. M10600000238). J.S.K. acknowledges the support by the KRF (Grant No. KRF-2006-311-C00277). This work has also benefited from the use of NPDF at the Lujan Center at Los Alamos Neutron Science Center, funded by DOE Office of Basic Energy Sciences. Los Alamos National Laboratory is operated by Los Alamos National Security LLC under DOE Contract No. DE-AC52-06NA25396. The upgrade of NPDF was funded by NSF through Grant No. DMR 00-76488. We also acknowledge the support of the National Institute of Standards and Technology, U.S. Department of Commerce, in providing the neutron research facilities used in this work.

*jaehc@korea.ac.kr

[1] R. Coldea, D. A. Tennant, A. M. Tsvelik, and Z. Tylczynski, Phys. Rev. Lett. **86**, 1335 (2001).

[2] K. Takada, H. Sakurai, E. Takayama-Muromachi, F. Izumi, R. A. Dilanian, and T. Sasaki, Nature (London) **422**, 53 (2003).

[3] T. Kimura, J. C. Lashley, and A. P. Ramirez, Phys. Rev. B **73**, 220401(R) (2006).

[4] M. Holzapfel, S. de Brion, C. Darie, P. Bordet, E. Chappel, G. Chouteau, P. Strobel, A. Sulpice, and M. D. Núñez-Regueiro, Phys. Rev. B **70**, 132410 (2004).

[5] S. de Brion, C. Darie, M. Holzapfel, D. Talbayev, L. Mihály, F. Simon, A. Jánossy, and G. Chouteau, Phys. Rev. B **75**, 094402 (2007).

[6] A. Rougier, C. Delmas, and A. V. Chadwick, Solid State Commun. **94**, 123 (1995).

[7] J.-H. Chung, Th. Proffen, S. Shamoto, A. M. Ghorayeb, L. Croguennec, W. Tian, B. C. Sales, R. Jin, D. Mandrus, and T. Egami, Phys. Rev. B **71**, 064410 (2005).

[8] H. Yoshizawa, H. Mori, K. Hirota, and M. Ishikawa, J. Phys. Soc. Jpn. **59**, 2631 (1990).

[9] A.-L. Barra, G. Chouteau, A. Stepanov, and C. Delmas, J. Magn. Magn. Mater. **177-181**, 783 (1998).

[10] Y. Kitaoka, T. Kobayashi, A. Kōda, H. Wakabayashi, Y. Niino, H. Yamakage, S. Taguchi, K. Amaya, K. Yamaura, M. Takano, A. Hirano, and R. Kanno, J. Phys. Soc. Jpn. **67**, 3703 (1998).

[11] F. Reynaud, D. Mertz, F. Celestini, J.-M. Debierre, A. M. Ghorayeb, P. Simon, A. Stepanov, J. Voiron, and C. Delmas, Phys. Rev. Lett. **86**, 3638 (2001).

[12] J.-S. Kang, S. S. Lee, G. Kim, H. J. Lee, H. K. Song, Y. J. Shin, S. W. Han, C. Hwang, M. C. Jung, H. J. Shin, B. H. Kim, S. K. Kwon, and B. I. Min, Phys. Rev. B **76**, 195122 (2007).

[13] E. Wawrzyńska, R. Coldea, E. M. Wheeler, I. I. Mazin, M. D. Johannes, T. Sörgel, M. Jansen, R. M. Ibberson, and P. G. Radaelli, Phys. Rev. Lett. **99**, 157204 (2007).

[14] E. Wawrzyńska, R. Coldea, E. M. Wheeler, T. Sörgel, M. Jansen, R. M. Ibberson, P. G. Radaelli, and M. M. Koza, Phys. Rev. B **77**, 094439 (2008).

[15] Y. J. Shin, J. P. Doumerc, P. Dordor, C. Delmas, M. Pouchard, and P. Hagenmuller, J. Solid State Chem. **107**, 303 (1993).

[16] A. C. Larson and R. B. Von Dreele, General Structure Analysis System (GSAS), Los Alamos National Laboratory Report LAUR 86-748 (1994) .

[17] T. Egami and S. J. L. Billinge, *Underneath the Bragg Peaks: Structural Analysis of Complex Materials* (Pergamon, Amsterdam, 2003).

[18] C. L. Farrow, P. Juhas, J. W. Liu, D. Bryndin, E. S. Božin, J. Bloch, Th. Proffen, and S. J. L. Billinge, J. Phys.: Condens. Matter **19**, 335219 (2007).

[19] W. Sikora, F. Bialas, and L. Pytlik, J. Appl. Crystallogr. **37**, 1015 (2004).

[20] L. D. Dyer, B. S. Borie Jr., and G. P. Smith, J. Am. Chem. Soc. **76**, 1499 (1954).

[21] For simplicity of discussions, we do not distinguish Ni3 from Ni2. Otherwise, the symmetry will be lower than $C2/m$.

[22] H. Kikuchi, H. Nagasawa, M. Mekata, Y. Fudamoto, K. M. Kojima, G. M. Luke, Y. J. Uemura, H. Mamiya, and T. Naka, Hyperfine Interact. **120-121**, 623 (1999).